

Exploring Primordial Black Holes and Gravitational Waves with R-Symmetric GUT Higgs Inflation

Nadir Ijaz ^{1,*} and Mansoor Ur Rehman ^{1,†}

¹*Department of Physics, Quaid-i-Azam University, Islamabad 45320, Pakistan*

(Dated: February 22, 2024)

This study investigates the realization of R-symmetric Higgs inflation within the framework of no-scale-like supergravity, aiming to elucidate the formation of primordial black holes and observable gravitational waves within a class of GUT models. We explore the possibility of an ultra-slow-roll phase in a hybrid inflation framework, where the GUT Higgs field primarily takes on the role of the inflaton. The amplification of the scalar power spectrum gives rise to scalar-induced gravitational waves and the generation of primordial black holes. The predicted stochastic gravitational wave background falls within the sensitivity range of existing and upcoming gravitational wave detectors, while primordial black holes hold the potential to explain the abundance of dark matter. Furthermore, we highlight the significance of the leading-order nonrenormalizable term in the superpotential of achieving inflationary observables consistent with the latest experimental data. Additionally, the predicted range of the tensor-to-scalar ratio, a key measure of primordial gravitational waves, lies within the observational window of future experiments searching for B-mode polarization patterns in cosmic microwave background data.

I. INTRODUCTION

The detection of gravitational waves by experiments such as LIGO and Virgo [1–5] has opened up new avenues for investigating primordial black holes (PBHs) [6–10]. Most recently, the 15-year pulsar timing data collected by the North American Nanohertz Observatory for Gravitational Waves (NANOGrav) presented convincing evidence for a low-frequency Gravitational Wave Background (GWB) [11], potentially originating from PBHs [12]. Future space-based GW interferometers like LISA, BBO, and DECIGO [13, 14] are anticipated to detect similar background signals. PBHs have been proposed as potential constituents of dark matter, accounting for anywhere from a fraction to the entirety of its abundance. One of the primary mechanisms for PBH formation in the early universe involves the amplification of the primordial curvature perturbation spectrum. The mass of these PBHs is intricately linked to the Hubble mass, representing the mass energy contained within a Hubble sphere at the time of PBH formation. Consequently, PBHs offer a plausible explanation for a diverse range of cosmic phenomena [15–20].

In the vast landscape of cosmology, inflation emerges as a crucial concept that sheds light on fundamental characteristics of the observable universe at large scales. Inflation explains critical aspects of the universe’s structure, such as its immense size, uniformity, isotropy, and overall geometry. It gives rise to primordial density fluctuations, acting as the foundational “seeds” for the creation of the cosmic structures we observe today, including galaxies and galaxy clusters. These primordial density fluctuations, in the standard inflationary scenario, originate

from quantum fluctuations of a scalar field during the inflationary epoch. Additionally, inflation triggers the amplification of tensor perturbations in the spacetime metric, resulting in the generation of primordial gravitational waves.

Given the effectiveness of cosmic inflation in elucidating the early universe, it’s pertinent to consider inflation as a mechanism for magnifying the primordial power spectrum. Beyond the formation of primordial black holes, the amplified perturbations in scalar curvature are expected to yield significant secondary tensor perturbations. These aspects have been investigated in recent studies [21–33].

In the quest to establish a ‘standard model of inflationary cosmology,’ supersymmetric hybrid inflation (SHI) [34–39] provides an elegant framework for integrating grand unified theories (GUTs) of particle physics [40]. Previous studies have explored the formation of PBHs within SHI, employing R-symmetry breaking terms in the Kähler potential [33, 41]. Similar models have also been investigated in [27]. This paper investigates the formation of PBHs in an R-symmetric SHI framework for a generic GUT model, without introducing any R-symmetry violating terms in either the superpotential or the Kähler potential. We adopt a no-scale-like supergravity-based framework, where the GUT Higgs field primarily functions as the inflaton. A multifield treatment is necessary for PBH formation. To achieve inflationary observables consistent with observational constraints, we also consider the leading-order nonrenormalizable term in the superpotential.

The paper is structured as follows: Section II provides an overview of the R-Symmetric Higgs inflation within a generic GUT model, focusing on its formulation within a no-scale-like supergravity framework. In Section III, we delve into the effective single-field treatment of the model. Section IV extends the analysis to include the multifield treatment, exploring the presence of

* nadirijaz1919@gmail.com

† mansoor@qau.edu.pk

PBHs and gravitational waves, with particular attention given to the role of the leading-order nonrenormalizable term in the superpotential. We highlight the parametric range where observable inflationary primordial gravitational waves are expected, along with a brief discussion on successful reheating and leptogenesis scenarios. Additionally, we touch upon the potential of PBHs as dark matter and their relevance in explaining NanoGrav observations. Finally, Section V presents our conclusions.

II. R-SYMMETRIC HIGGS INFLATION

We consider an R-symmetric superpotential of the form,

$$W = \kappa S (H^2 - M^2) + \beta SH^3, \quad (1)$$

where κ and β are dimensionless coupling, and M is some mass scale. The parameter β can in general be complex but we assume it to be real and positive similar to κ and M . The R-charge of the H -superfield is zero, and the R-charge of the S -superfield is identical to that of the superpotential W . The superpotential presented above has previously been utilized in shifted hybrid inflation models [42], where the scalar component of the gauge singlet field S serves as the inflaton, while the GUT Higgs field remains stabilized at a local minimum during inflation. However, in the current investigation, these roles will be reversed, with the GUT Higgs field primarily assuming the role of the inflaton.

The above form of superpotential can elegantly incorporate several GUT models listed below:

- $SU(5)$ or $SU(5) \times U(1)$ where H belongs to the adjoint representation 24 [33, 42–45].
- $SU(4)_c \times SU(2)_L \times U(1)_R$ where H can be identified with the adjoint representation 15 [46].

While dealing with conjugate pair of GUT Higgs fields ($H \oplus \bar{H}$), the terms, κSH^2 and βSH^3 , in the above superpotential are replaced by $\kappa SH\bar{H}$ and $\beta S(H\bar{H})^2$:

- $SO(10)$ with $16 \oplus \bar{16}$ [47].
- $SU(3)_c \times SU(2)_L \times SU(2)_R \times SU(1)_{B-L}$ with $(1, 1, 2, 1) \oplus (1, 1, 2, -1)$ [48]
- Flipped $SU(5) \equiv SU(5) \times U(1)$ with $(10, 1) \oplus (\bar{10}, -1)$ [39, 43, 49–52].
- $SU(3)_c \times SU(2)_L \times U(1)_Y \times U(1)_{B-L}$ with $(1, 1, 0, 1) \oplus (1, 1, 0, -1)$ [53, 54].

To realize non-minimal inflation we consider a Kähler potential of the form $K = -3 \ln \Phi$, where

$$\Phi = 1 - \frac{1}{3}(|S|^2 + |H|^2) + \frac{\chi}{4}(H^2 + h.c.) + \frac{\gamma_4}{3}|S|^4 + \frac{\gamma_6}{3}|S|^6. \quad (2)$$

Here χ , γ_4 and γ_6 are dimensionless parameters and the reduced Planck mass, $m_P = 2.4 \times 10^{18}$ GeV, is set to unity. The quartic term is usually employed to stabilize the S field at the origin during inflation [55]. As discussed below, the sextic term plays an important role in generating primordial black holes. It's important to note that each term within the Kähler potential preserves the R-symmetry, unlike models where primordial black holes are formed with a cubic term in the Kähler potential, albeit at the cost of R-symmetry breaking at nonrenormalizable level [33].

The scalar-gravity portion of the Lagrangian is expressed in the following manner

$$\mathcal{L}_J = \sqrt{-g_J} \left[\frac{\Phi \mathcal{R}_J}{2} - g_J^{\mu\nu} \mathcal{G}_{ij} \partial_\mu z^i \partial_\nu z^{*j} - V_J \right], \quad (3)$$

where $g_J^{\mu\nu}$ is the inverse of the Jordan frame spacetime metric $g_{\mu\nu}^J$, \mathcal{R}_J is the Ricci scalar in the Jordan frame, V_J represents the scalar potential in the Jordan frame, and $z_i \in \{H, S\}$. The metric on the field-space manifold in the Jordan frame, \mathcal{G}_{ij} , is defined as

$$\mathcal{G}_{ij} \equiv -3 \frac{\partial^2 \Phi}{\partial z_i \partial z_j^*}. \quad (4)$$

The fields S and H can be written in the form,

$$S = \frac{1}{\sqrt{2}} s e^{i\theta_s}, \quad H = \frac{1}{\sqrt{2}} h e^{i\theta_h}, \quad (5)$$

where s and h are the real canonically normalized scalar fields. Here and below same notation has been used for the superfields and their scalar components. Assuming the phases, (θ_s, θ_h) , to be stabilized at zero, the above Lagrangian becomes

$$\mathcal{L}_J = \sqrt{-g_J} \left[\frac{\Phi \mathcal{R}_J}{2} - \frac{1}{2} g_J^{\mu\nu} \partial_\mu h \partial_\nu h - \frac{\zeta}{2} g_J^{\mu\nu} \partial_\mu s \partial_\nu s - V_J \right], \quad (6)$$

where

$$\zeta = 1 - 2\gamma_4 s^2 - \frac{9}{4} \gamma_6 s^4, \quad (7)$$

and

$$\Phi = 1 - \frac{s^2}{6} + \frac{\gamma_4}{12} s^4 + \frac{\gamma_6}{24} s^6 + \xi h^2, \quad (8)$$

with

$$\xi \equiv \frac{\chi}{4} - \frac{1}{6}. \quad (9)$$

We then proceed with a conformal transformation of the spacetime metric, to work in the Einstein frame

$$g_{\mu\nu}^E = \Phi g_{\mu\nu}^J. \quad (10)$$

This transformation leads to the following Lagrangian in the Einstein frame with a canonical coupling to gravity:

$$\mathcal{L}_E = \sqrt{-g_E} \left[\frac{1}{2} \mathcal{R}_E - \frac{1}{2} G_{ij} g_E^{\mu\nu} \partial_\mu z^i \partial_\nu z^{*j} - V_E \right], \quad (11)$$

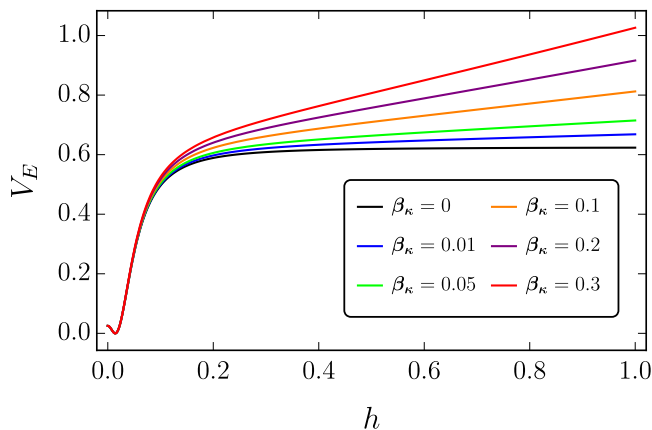


FIG. 1. The normalized Einstein frame potential at $s = 0$ for $M \simeq 10^{16}$, $\xi = 10^3$, $\gamma_4 = 0.01$ and different values of β_κ , where $\beta_\kappa = \beta/\kappa$.

where in the Einstein frame, the kinetic term for the scalar fields incorporates a field-space metric [56, 57],

$$G_{ij} = \frac{1}{\Phi} \left[\mathcal{G}_{ij} + \frac{3}{2} \frac{\Phi_{,i} \Phi_{,j}}{\Phi} \right], \quad (12)$$

where $\Phi_{,i} \equiv \partial\Phi/\partial z^i$. Along the D-flat direction, the supergravity (SUGRA) scalar potential in the Einstein frame, $V_E = \Phi^{-2} V_J$, is defined as,

$$V_E = e^{K/m_P^2} \left(K_{ij} D_{z_i} W D_{z_j} W^* - 3m_P^{-2} |W|^2 \right), \quad (13)$$

where,

$$D_{z_i} W \equiv \frac{\partial W}{\partial z_i} + m_P^{-2} \frac{\partial K}{\partial z_i}, \quad K_{ij} \equiv \frac{\partial^2 K}{\partial z_i \partial z_j^*}, \quad (14)$$

$D_{z_i}^* W^* = (D_{z_i} W)^*$ and $K = -3 \ln \Phi$. For the background equations and the relevant power spectra in a multifield framework, see Refs. [57–62].

III. EFFECTIVE SINGLE FIELD INFLATION

The field S can be stabilized at zero which becomes a minimum with a vanishing γ_6 and a suitable nonzero value of γ_4 . We thus obtain an effective Higgs potential which, for field values below m_P , can be employed to realize nonminimal Higgs inflation. This effective potential has been previously analyzed in great detail in [33, 52]. Also, see [63] for a generalized treatment with Z_n symmetry. In the present work, we aim to study the impact of leading order non-renormalizable term with parameter β in the superpotential on inflationary observables.

With s stabilized at the origin, the scalar potential in the Einstein frame takes the following form

$$V_E = \frac{1}{16} \frac{(2\kappa h^2 - 4\kappa M^2 + \sqrt{2}\beta h^3)^2}{(1 + \xi h^2)^2}. \quad (15)$$

For $N_0 = 50$			
β_κ	κ	n_s	r
0	0.0053	0.961	0.0043
0.01	0.0055	0.964	0.0046
0.02	0.0057	0.966	0.0051
0.05	0.0065	0.974	0.0066
For $N_0 = 60$			
0	0.0044	0.968	0.0030
0.01	0.0047	0.971	0.0034
0.02	0.0049	0.973	0.0038
0.03	0.0052	0.976	0.0042

TABLE I. The predicted values of inflationary parameters with gauge symmetry breaking scale $M = 0.01$, $\xi = 10^3$, $\gamma_4 = 0.01$ and $\gamma_6 = 0$.

The effect of β on the scalar potential is shown in Fig. 1 for fixed values of $\gamma_4 = 0.01$, $\xi = 10^3$ and $M = 0.01$. An increase in the potential's slope is observed which is expected to introduce intriguing effects on the predictions of inflationary observables, as elaborated below.

After conformal rescaling the canonically normalized inflaton field $\hat{h}(h)$ in the Einstein frame becomes a function of field h as

$$J(h) \equiv \left(\frac{d\hat{h}}{dh} \right) = \sqrt{\frac{1}{\Phi} + \frac{3}{2} \left(\frac{d \ln \Phi}{dh} \right)}. \quad (16)$$

The slow-roll parameters can now be expressed in terms of h as

$$\epsilon(h) = \frac{1}{2} \left(\frac{V'_E}{J V_E} \right)^2, \quad \eta(h) = \left(\frac{V''_E}{J^2 V_E} - \frac{J' V'_E}{J^3 V_E} \right), \quad (17)$$

where a prime denotes a derivative with respect to h . The scalar spectral index n_s and the tensor to scalar ratio r to the first order in slow-roll approximation are given by

$$n_s \simeq 1 - 6\epsilon(h_0) + 2\eta(h_0), \quad r \simeq 16\epsilon(h_0), \quad (18)$$

where the field value, h_0 , corresponds to the number of e-folds,

$$N_0 = \frac{1}{\sqrt{2}} \int_{h_e}^{h_0} \frac{J(h)}{\sqrt{\epsilon(h)}} dh, \quad (19)$$

before the end of inflation at $h = h_e$ defined by the condition $\epsilon(h_e) = 1$. Also, h_0 corresponds to the pivot scale where the amplitude of the scalar power spectrum is normalized by Planck [64] to be,

$$A_s(k_0) = \frac{V_E(h)}{24\pi\epsilon(h)} \Big|_{h(k_0)=h_0} = 2.137 \times 10^{-9}, \quad (20)$$

at $k_0 = 0.05 \text{ Mpc}^{-1}$.

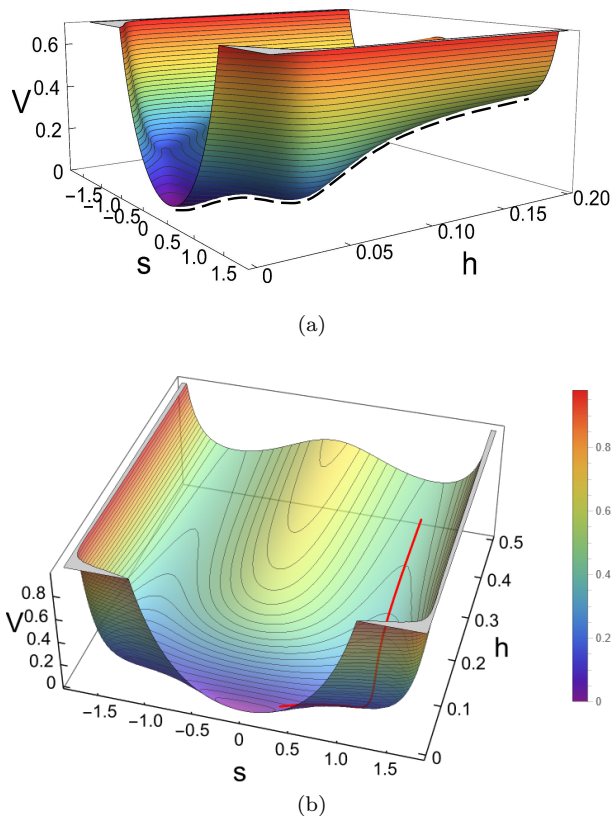


FIG. 2. (a) The inflection point is depicted in the 3D Einstein frame potential. (b) The inflationary trajectory (red) superimposed on the Einstein frame potential.

Using eqs. (15), and (17), the slow-roll parameters in the large ξ limit and leading order in β are given by

$$\begin{aligned} \epsilon &\simeq \frac{4}{3\psi^4} + \frac{2\beta_\kappa}{3\psi} \sqrt{\frac{2}{\xi}}, \\ \eta &\simeq -\frac{4}{3\psi^2} + \frac{\beta_\kappa}{3} \sqrt{\frac{1}{2\xi}} \psi. \end{aligned} \quad (21)$$

Here, $\psi \equiv \sqrt{\xi}h$ is a dimensionless field variable taking the value at the pivot scale approximated as $\psi_0 \simeq \sqrt{4N_0/3}$ and at the end of inflation as $\psi_e \simeq (4/3)^{1/4} < \psi_0$. The spectral index and tensor-to-scalar ratio are then expressed as,

$$\begin{aligned} n_s &\simeq 1 - \frac{8}{3\psi_0^2} + \frac{2\beta_\kappa}{3} \frac{\psi_0}{\sqrt{2\xi}} \simeq 1 - \frac{2}{N_0} + \frac{2\beta_\kappa}{3} \sqrt{\frac{2N_0}{3\xi}}, \\ r &\simeq \frac{12}{N_0^2} + 16\beta_\kappa \sqrt{\frac{2}{3N_0\xi}}. \end{aligned} \quad (22)$$

These analytical expressions elucidate how the scalar spectral index (n_s) and the tensor-to-scalar ratio r rise with increasing β . The influence of the parameter β is detailed in Table I for 50 and 60 e-folds, with a fixed value of $M = 0.01$. This role of β also proves instrumental in attaining observationally consistent values of

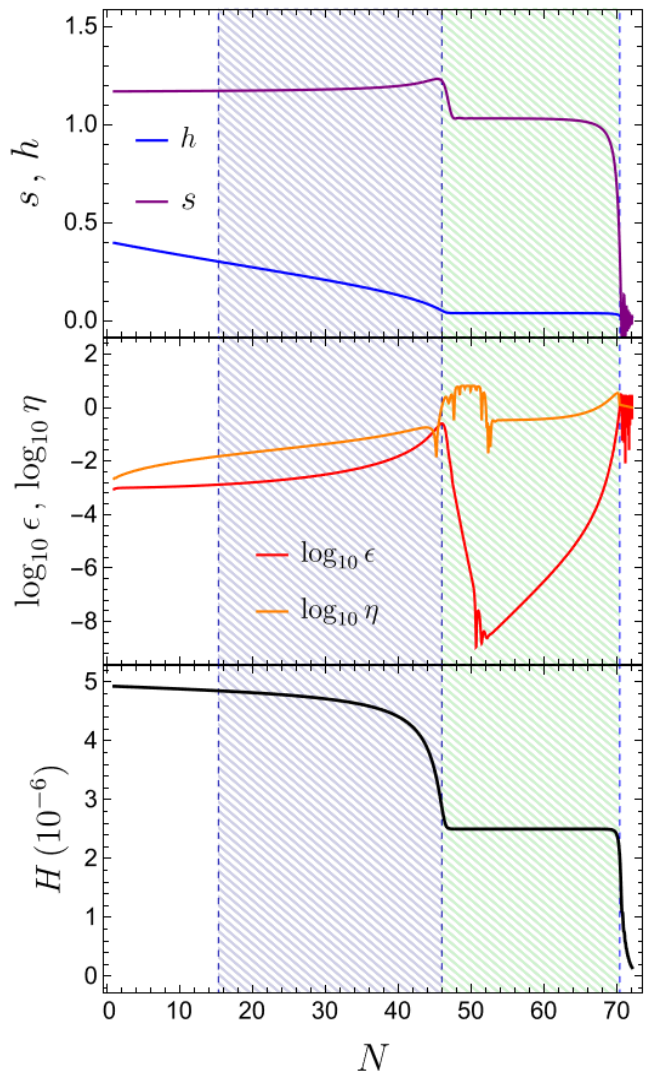


FIG. 3. From top to bottom we show as a function of the number of e-folds, the dynamics of the fields, the slow-roll parameters (ϵ and η), and the Hubble parameter H . The blue-hatched region represents the first stage of inflation, and the green-hatched region represents the second stage.

the scalar spectral index within the multifield scenario, as elaborated in the subsequent section.

IV. MULTIFIELD INFLATION

Setting γ_6 to zero enabled us to achieve effective single-field inflation, as investigated in the preceding section. However, in this section, we introduce a non-zero γ_6 . For $\gamma_6 > 0$ and $\gamma_4 < 0$, two additional local minima emerge at non-zero values of the s -field for $\xi \gg 1$ and $h \gg M$, given approximately by:

$$s_{\min} \simeq \pm \frac{2}{3} \sqrt{-\frac{\gamma_4}{\gamma_6}}. \quad (23)$$

With $\gamma_4 < 0$, the $s = 0$ trajectory transforms into a local maximum for $h \gg M$. The significance of γ_4 is evident from the expression above, as it can shift the positioning of the local minimum (valley) of the potential towards larger s -field values at $h \gg M$ for a fixed γ_6 . By selecting suitable values for γ_6 and γ_4 , a region of false vacuum can be established near an effective inflection point in the potential [27]. This is the region where a phase of Ultra Slow Roll (USR) inflation can be realized. In Fig. 2a, we illustrate a 3D representation of the Einstein frame potential, showcasing the presence of this inflection point region. By appropriately tuning γ_6 and γ_4 , the depth of this false vacuum can be modified. For our numerical computations, we utilized the multifield formalism tools as described in Refs.[57–62].

In Fig. 2b, we present the inflationary trajectory superimposed on the Einstein frame potential, where $\gamma_6 = 0.13$ and $\gamma_4 = -0.395804$. The evolution of the fields is depicted in the top panel of Fig. 3. This trajectory undergoes two distinct stages: initially, it experiences typical slow-roll inflation within the valley, and upon reaching the inflection point, a second stage of Ultra Slow Roll (USR) inflation begins. During USR, the first slow-roll parameter, $\epsilon = -\dot{H}/H^2$, is significantly suppressed ($\epsilon_{USR} \ll \epsilon_{SR}$). We identify the end of the first stage from the local maximum of ϵ (or when $\eta \equiv 2\epsilon - \dot{\epsilon}/2H\epsilon$ first crosses unity). Inflation ends when the parameter ϵ attains unity, as depicted in the middle panel of Fig. 3. The blue-hatched region signifies the first stage of inflation, while the green-hatched region represents the second stage. The duration of USR can be regulated by adjusting the parameter γ_4 while keeping γ_6 fixed. The Hubble parameter is presented in the bottom panel of Fig.3.

A. The Role of β Parameter

The USR phase induces an enhancement of the scalar power spectrum. However, when $\beta = 0$, prolonging the USR phase causes a shift in the scalar spectral index towards lower values and the tensor-to-scalar ratio towards larger values, moving away from the central range preferred by the Planck data. Table II demonstrates how, for a fixed γ_6 , the parameter γ_4 governs the duration of the USR phase and its corresponding predictions for inflationary observables.

In our numerical analysis in this section, we set the reheating temperature at 10^9 GeV, resulting in approximately 55 e-folds of inflation. The power spectrum of curvature perturbations is computed numerically using a publicly available Mathematica package [65] based on the transport method [66, 67]. Fig. 4 illustrates the power spectrum for the points listed in Table II. We utilize the parameter κ to normalize the power spectrum to the observed value (Eq. 20) by Planck [64]. It's worth noting that for the case where $\beta = 0$, although an enhancement in the power spectrum can be achieved, the scalar spec-

tral index deviates from the observationally preferred $1-\sigma$ region.

As demonstrated in Section III, the parameter β exerts a significant effect by shifting the spectral index towards a more favored region. This prompts us to explore its potential to attain observationally consistent results for inflationary observables. Thus, we examine four Benchmark Points (BP) listed in Table III, each featuring non-zero values of β , and present the resulting power spectra in Fig. 5. We incorporate constraints on the power spectrum from Planck [64], Lyman-alpha [68], and FIRAS μ -distortions measurements [69]. For a comprehensive investigation into spectral distortions in both single and multifield inflation scenarios, see Ref. [70].

As illustrated in Table III, leveraging non-zero values of β allows us to readily attain scalar spectral index values within the $1-\sigma$ bound of Planck data. This underscores the significance of the tensor-to-scalar ratio achieved within this model, a point further elaborated upon in the subsequent subsection.

B. Primordial Gravitational Waves

An important contributor to the stochastic gravitational wave background arises from the quantum fluctuations of the spacetime metric itself. While these tensor perturbations undergo amplification during inflation, direct detection remains challenging; nevertheless, they leave distinct imprints on the CMB spectrum via B-mode polarization. The tensor-to-scalar ratio, r , serves as a fundamental metric for these primordial gravitational waves, constrained from above by current CMB observations to $r \leq 0.036$ at a 95% confidence level [71]. Future experiments are poised to explore the observable range, $0.001 \lesssim r \lesssim 0.04$ [72–74]. Depending on the value of β , our model predicts the tensor-to-scalar ratio in the range, $0.02 \lesssim r \lesssim 0.04$. This range is consistent with the $1-\sigma$ bound on n_s and remains detectable by future experiments. Note that the effective single-field treatment, where primordial black hole production is not considered, yields a lower value for r , potentially as low as 0.003, a typical prediction of the Starobinski inflationary model. The Benchmark Point (BP-4) listed in Table III predicts a value of $r \simeq 0.1$, which falls beyond the $2-\sigma$ bound of Planck data. Nonetheless, its significance will be addressed in the final subsection.

C. Reheating and Leptogenesis

Following the end of inflation, the inflaton begins oscillating around the global minimum defined by:

$$\langle S \rangle = 0, \langle H^2 - M^2 + \beta_\kappa H^3 \rangle = 0, \quad (24)$$

where $\langle H \rangle \approx M$ within the relevant parametric range. The oscillating inflaton is composed of two complex

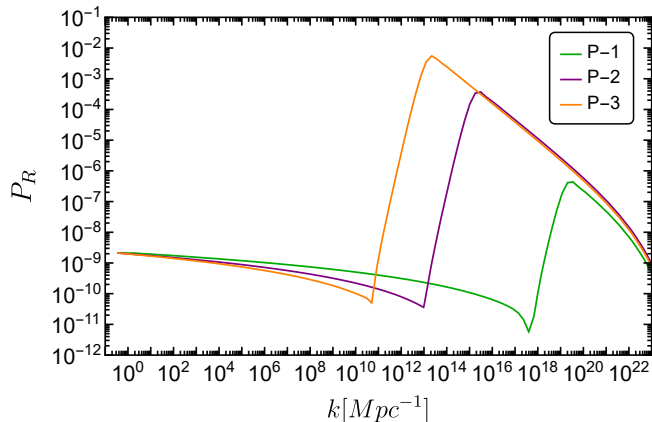


FIG. 4. Power spectrum of scalar perturbations, P_R , as a function of the comoving wavenumber k computed numerically for points in Table II

	γ_6	γ_4	ΔN_2	n_s	r
P-1	0.13	-0.394700	12	0.956	0.0059
P-2	0.13	-0.394830	21	0.944	0.0095
P-3	0.13	-0.394835	26	0.935	0.0126

TABLE II. Points for $\beta = 0$, a fixed γ_6 and three different values of γ_4 , showing how the parameter γ_4 controls the duration of the USR phase (ΔN_2). The spectral index in this is inconsistent with the observational data and decreases with the increase in the duration of the USR phase. The scalar power spectrum for these points is shown in Fig. 4

scalar fields S and H , both possessing a common mass. During this phase, the inflaton can decay into the lightest right-handed neutrino, N , through

$$W \supset \frac{\gamma_{ij}}{m_P} H^2 N_i N_j \supset M_{ij}^R N_i N_j, \quad (25)$$

where $M_{ij}^R \sim \gamma_{ij} \langle H^2 \rangle / m_P$ constitutes the mass matrix for right-handed neutrinos, and N represents the field with the lightest mass eigenvalue. Note that this term respects R-symmetry, with N_i carrying an R-charge of one. After the reheating process, the lepton asymmetry generated by inflaton decay undergoes partial conversion to baryon asymmetry via sphaleron processes [75, 76]. To circumvent the issue of gravitino overproduction, as previously discussed, the reheating temperature is fixed at 10^9 GeV. With this chosen reheating temperature, the observed baryon asymmetry can also be accounted for [33].

D. Abundance of Primordial Black Holes

During horizon reentry, the enhanced curvature perturbations can cause the formation of PBHs through gravitational collapse. Our focus in this section is to compute the mass of PBHs and their fractional energy

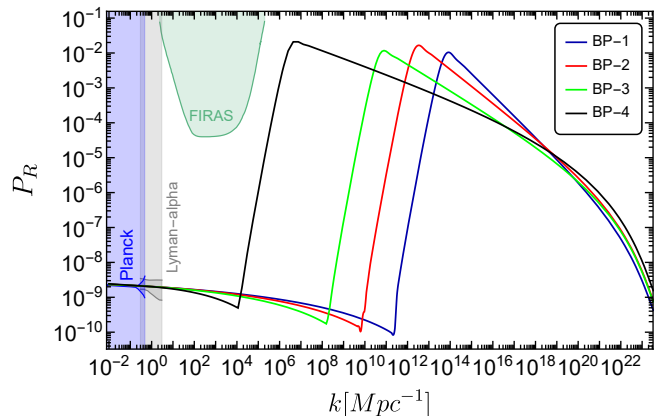


FIG. 5. Power spectrum of scalar perturbations, P_R , as a function of the comoving wavenumber k computed numerically for benchmark points in Table III. The shaded regions are excluded by Planck [64], Lyman-alpha [68], and FIRAS μ -distortions measurements [69].

	γ_6	γ_4	β_κ	n_s	r
BP-1	0.13	-0.395804	0.12	0.965	0.021
BP-2	0.09	-0.301128	0.16	0.964	0.028
BP-3	0.065	-0.235523	0.22	0.964	0.040
BP-4	0.04	-0.1631133	0.65	0.963	0.100

TABLE III. The Benchmark Points (BP) we used for our numerical analysis, along with the predictions for the inflationary observable n_s and r . Here the first benchmark point has the same γ_6 as in table II.

density abundances, assuming they are formed during the radiation-dominated epoch.

When the perturbation associated with the PBH enters the horizon, the PBH's mass is dictated by the horizon's mass. The relationship between the scale of the perturbation and the mass of the PBH during formation is expressed as follows,

$$M_{PBH} = \gamma M_{H,0} \Omega_{rad,0}^{1/2} \left(\frac{g_{*,0}}{g_{*,f}} \right)^{1/6} \left(\frac{k_0}{k_f} \right)^2, \quad (26)$$

where $M_{H,0} = \frac{4\pi}{H}$ represents the mass of horizon, Ω_{rad} is used to denote the energy density parameter for radiation, while g_* represents the effective degrees of freedom. The subscripts f and 0 correspond to the time of formation and the present day respectively. The ratio between the PBH mass and the horizon mass is denoted by γ , which is estimated to be $\gamma \simeq 3^{-3/2}$, in the simple analytical result [77]. The energy density of the PBHs at present can be determined by redshifting it at the formation time. This means that $\rho_{PBH,0} = \rho_{PBH,f} (a_f/a_0)^3 \approx \gamma \beta \rho_{rad,f} (a_f/a_0)^3$, as the PBHs act like matter. Here β denotes the mass fraction of the Universe collapsing in PBH mass.

The Press-Schechter method is used to evaluate the mass fraction β assuming that the overdensity δ follows

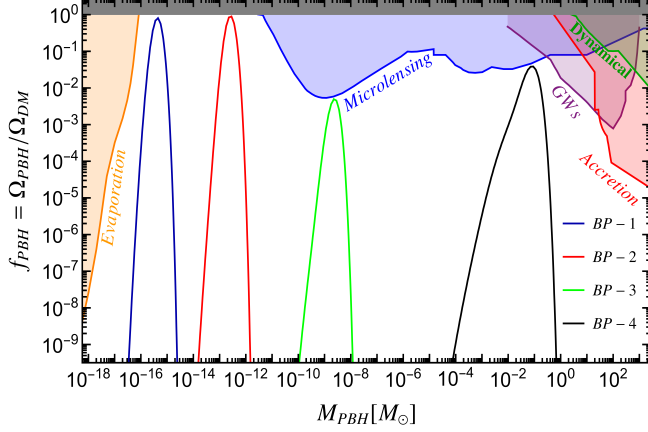


FIG. 6. Fraction of dark matter in the form of PBHs with mass M_{PBH} . For the various constraints see Ref. [17] and for an updated repository of data see [📄/bradkav/PBHbounds](https://github.com/bradkav/PBHbounds).

a gaussian probability distribution function. The collapse of PBH is determined by a threshold value denoted as δ_c . Thus, the mass fraction can be expressed as

$$\beta = \int_{\delta_c}^{\infty} d\delta \frac{1}{\sqrt{2\pi\sigma^2}} \exp\left(-\frac{\delta^2}{2\sigma^2}\right), \quad (27)$$

where σ is the variance of curvature perturbation that is related to the co-moving wavenumber [78].

$$\sigma^2 = \frac{16}{81} \int_0^{\infty} d\ln q (qk^{-1})^4 W^2(qk^{-1}) \mathcal{P}_\zeta(q), \quad (28)$$

where $W^2(qk^{-1})$ is a window function that we approximate with a Gaussian distribution function,

$$W(qk^{-1}) = \exp\left[-\frac{1}{2}(qk^{-1})^2\right]. \quad (29)$$

For δ_c we assume values in the range between 0.4 and 0.6 [79–84].

The total abundance is $\Omega_{PBH,tot} = \int d\ln M_{PBH} \Omega_{PBH}$, with Ω_{PBH} expressed in terms of f_{PBH} which is given by,

$$\begin{aligned} f_{PBH} &\equiv \frac{\Omega_{PBH,0}}{\Omega_{CDM,0}} \\ &\approx \left(\frac{\beta(M)}{8.0 \times 10^{-15}}\right) \left(\frac{0.12}{\Omega_{CDM,0} h^2}\right) \left(\frac{\gamma}{0.2}\right)^{3/2} \\ &\times \left(\frac{106.75}{g_{*,f}}\right)^{1/4} \left(\frac{M_{PBH}}{10^{20} \text{g}}\right)^{-\frac{1}{2}}, \end{aligned} \quad (30)$$

where $\Omega_{CDM,0}$ is the today's density parameter of the cold dark matter and h is the rescaled Hubble rate today. The fractional abundance of the primordial black holes as a function of their mass is shown in Fig. 6. We have used the benchmark point parameters of table III. For only the first two BPs, the PBHs can explain dark matter in totality. The shaded regions correspond to the various observational constraints [17, 85, 86].

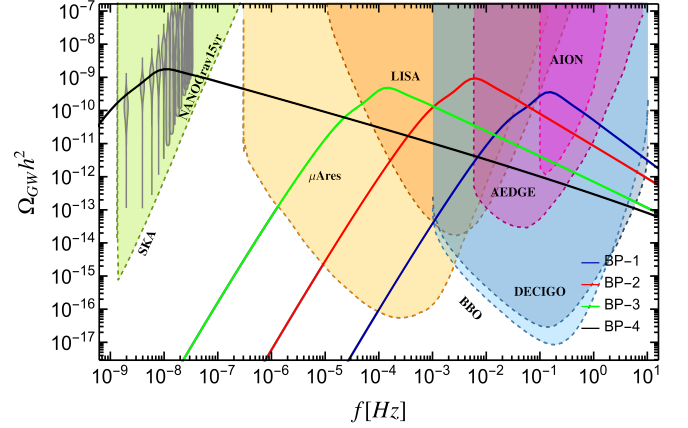


FIG. 7. Fraction of the energy density in GWs relative to the critical energy density of the universe as a function of the frequency. We show the sensitivity curves of: AION [87], AEDGE [88], DECIGO [89, 90], BBO [91], LISA [13], μ -Ares [92], SKA [93, 94] and the gray violins are the NANOGrav frequency bins [12]. We use as a comparison the first 15 bins of the NANOGrav 15 signal.

E. Scalar-induced gravitational wave

The GWs energy density within the subhorizon regions can be expressed as [95],

$$\rho_{GW} = \frac{\langle \partial_l h_{ij} \partial^l h^{ij} \rangle}{16a^2}, \quad (31)$$

here the average over oscillation is denoted by the overline and h_{ij} is the tensor mode. We can decompose h_{ij} as,

$$h_{ij}(t, \mathbf{x}) = \int \frac{d^3\mathbf{k}}{(2\pi)^{3/2}} (h_{\mathbf{k}}^+(t) e_{ij}^+(\mathbf{k}) + h_{\mathbf{k}}^\times(t) e_{ij}^\times(\mathbf{k})) e^{i\mathbf{k}\cdot\mathbf{x}}, \quad (32)$$

with $e_{ij}^+(\mathbf{k})$ and $e_{ij}^\times(\mathbf{k})$ being the polarization tensors and can be expressed as,

$$e_{ij}^+(\mathbf{k}) = \frac{1}{\sqrt{2}} (e_i(\mathbf{k}) e_j(\mathbf{k}) - \bar{e}_i(\mathbf{k}) \bar{e}_j(\mathbf{k})), \quad (33)$$

$$e_{ij}^\times(\mathbf{k}) = \frac{1}{\sqrt{2}} (e_i(\mathbf{k}) \bar{e}_j(\mathbf{k}) - \bar{e}_i(\mathbf{k}) e_j(\mathbf{k})), \quad (34)$$

here $e_i(\mathbf{k})$ and $\bar{e}_j(\mathbf{k})$ are orthogonal to each other. Expression (32) can be used in (31), which yields,

$$\rho_{GW}(t) = \int d\ln k \frac{\overline{\mathcal{P}_h(t, k)}}{2} \left(\frac{k}{2a}\right)^2. \quad (35)$$

In this expression $\mathcal{P}_h \equiv \mathcal{P}_h^{+,\times}$ and can be defined as,

$$\langle h_{\mathbf{k}}^+(t) h_{\mathbf{q}}^+(t) \rangle = \frac{2\pi^2}{k^3} \mathcal{P}_h^+(t, k) \delta^3(\mathbf{k} + \mathbf{q}), \quad (36)$$

$$\langle h_{\mathbf{k}}^\times(t) h_{\mathbf{q}}^\times(t) \rangle = \frac{2\pi^2}{k^3} \mathcal{P}_h^\times(t, k) \delta^3(\mathbf{k} + \mathbf{q}). \quad (37)$$

It should be noted that $\mathcal{P}_h^+(t, k) = \mathcal{P}_h^\times(t, k)$. The energy density parameter for gravitational wave is defined as follows,

$$\Omega_{\text{GW}}(t, k) \equiv \frac{\rho_{\text{GW}}(t, k)}{\rho_{\text{crit}}} = \frac{1}{24} \left(\frac{k}{aH} \right)^2 \overline{\mathcal{P}_h(t, k)}, \quad (38)$$

where we have omitted the polarization index.

The following tensor perturbation equation should be solved for obtaining the tensor power spectrum [96–98],

$$h''_{\mathbf{k}} + 2aHh'_{\mathbf{k}} + k^2 h_{\mathbf{k}} = 4S_{\mathbf{k}}, \quad (39)$$

where derivatives with respect to conformal time are denoted by the prime. The source term $S_{\mathbf{k}}$ is expressed as,

$$S_{\mathbf{k}} = \int \frac{d^3q}{\sqrt{(2\pi)^3}} q_i q_j e_{ij}(\mathbf{k}) \left[2\Phi_{\mathbf{q}} \Phi_{\mathbf{k}-\mathbf{q}} + \frac{4}{3+3\omega} \left(\frac{\Phi'_{\mathbf{q}}}{\mathcal{H}} + \Phi_{\mathbf{q}} \right) \left(\frac{\Phi'_{\mathbf{k}-\mathbf{q}}}{\mathcal{H}} + \Phi_{\mathbf{k}-\mathbf{q}} \right) \right], \quad (40)$$

the ω here is the equation of state. The generation of induced gravitational waves is assumed to occur during the radiation-dominated era. Thus, at the time of their generation, we have [97],

$$\begin{aligned} \Omega_{\text{GW}}(t_f, k) &= \frac{1}{12} \int_0^\infty dv \int_{|1-v|}^{1+v} du \left(\frac{4v^2 - (1+v^2 - u^2)^2}{4uv} \right)^2 \\ &\times \mathcal{P}_\zeta(ku) \mathcal{P}_\zeta(kv) \left(\frac{3(u^2 + v^2 - 3)}{4u^3 v^3} \right)^2 \\ &\times \left[\left(\pi^2 (-3 + v^2 + u^2)^2 \theta(-\sqrt{3} + u + v) \right) \right. \\ &\left. + \left(-4uv + (v^2 + u^2 - 3) \text{Log} \left| \frac{3 - (u+v)^2}{3 - (u-v)^2} \right| \right)^2 \right]. \end{aligned} \quad (41)$$

We can determine the energy density parameter for the current time as follows [97, 99],

$$\Omega_{\text{GW}} = \Omega_{\text{rad},0} \Omega_{\text{GW}}(t_f) \quad (42)$$

where we have multiplied $\Omega_{\text{GW}}(t_f)$ with the today radiation energy density parameter, $\Omega_{\text{rad},0}$.

Utilizing the numerically computed power spectrum of scalar perturbations, as depicted in Fig. 5, we derive the corresponding second-order gravitational wave (GW) spectrum. Our findings, illustrated in Fig. 7, represent the energy density fraction of gravitational waves relative to the critical energy density, denoted as Ω_{GW} . Our analysis reveals that the predictions for all four benchmark points (BPs) intersect the sensitivity thresholds of upcoming experiments. Notably, the prediction for the fourth BP (depicted by the black curve) is also consistent with the NanoGrav 15-year data. However, it's worth noting that the tensor-to-scalar ratio for this BP contradicts the observations from the Planck satellite. Consequently, the constraints imposed by the observational data on the tensor-to-scalar ratio hinder our model's ability to fully account for the NanoGrav observations.

V. CONCLUSION

We have successfully implemented GUT Higgs inflation within an R-symmetric hybrid framework based on no-scale supergravity. In the single-field treatment, our inflationary predictions for the scalar spectral index and the tensor-to-scalar ratio align closely with those of the Starobinski model, albeit with some variation. However, the multifield scenario presents a distinct prediction of observable primordial gravitational waves, with a larger tensor-to-scalar ratio falling within the detectable range of future experiments. The inclusion of the leading-order non-renormalizable term in the superpotential is crucial for ensuring the consistency of multifield predictions with Planck data. Additionally, our framework easily accommodates successful reheating and leptogenesis. An ultra-slow-roll phase is attainable within the multifield framework, leading to an enhancement of the scalar power spectrum. This enhancement facilitates the production of primordial black holes, offering a potential explanation for the abundance of dark matter. Lastly, the amplified scalar power spectrum gives rise to scalar-induced gravitational waves, which are detectable by both existing and forthcoming gravitational wave detectors.

[1] B. P. Abbott *et al.* (LIGO Scientific, Virgo), GW151226: Observation of Gravitational Waves from a 22-Solar-Mass Binary Black Hole Coalescence, *Phys. Rev. Lett.* **116**, 241103 (2016), [arXiv:1606.04855](https://arxiv.org/abs/1606.04855) [gr-qc].
 [2] B. P. Abbott *et al.* (LIGO Scientific, Virgo), GW170814: A Three-Detector Observation of Gravitational Waves from a Binary Black Hole Coalescence, *Phys. Rev. Lett.* **119**, 141101 (2017), [arXiv:1709.09660](https://arxiv.org/abs/1709.09660) [gr-qc].

[3] B. P. Abbott *et al.* (LIGO Scientific, Virgo), GW170608: Observation of a 19-solar-mass Binary Black Hole Coalescence, *Astrophys. J. Lett.* **851**, L35 (2017), [arXiv:1711.05578](https://arxiv.org/abs/1711.05578) [astro-ph.HE].
 [4] B. P. Abbott *et al.* (LIGO Scientific, VIRGO), GW170104: Observation of a 50-Solar-Mass Binary Black Hole Coalescence at Redshift 0.2, *Phys. Rev. Lett.* **118**, 221101 (2017), [Erratum: *Phys.Rev.Lett.* **121**, 129901 (2018)], [arXiv:1706.01812](https://arxiv.org/abs/1706.01812) [gr-qc].

- [5] B. P. Abbott *et al.* (LIGO Scientific, Virgo), Observation of Gravitational Waves from a Binary Black Hole Merger, *Phys. Rev. Lett.* **116**, 061102 (2016), [arXiv:1602.03837 \[gr-qc\]](#).
- [6] Y. B. Zel'dovich and I. D. Novikov, The Hypothesis of Cores Retarded during Expansion and the Hot Cosmological Model, *Soviet Astron. AJ (Engl. Transl.)*, **10**, 602 (1967).
- [7] S. Hawking, Gravitationally Collapsed Objects of Very Low Mass, *Monthly Notices of the Royal Astronomical Society* **152**, 75 (1971).
- [8] B. J. Carr and S. W. Hawking, Black Holes in the Early Universe, *Monthly Notices of the Royal Astronomical Society* **168**, 399 (1974).
- [9] B. J. Carr, The primordial black hole mass spectrum., *Astrophys. J.* **201**, 1 (1975).
- [10] M. I. Khlopov, B. A. Malomed, and I. B. Zeldovich, Gravitational instability of scalar fields and formation of primordial black holes, *Mon. Not. Roy. Astron. Soc.* **215**, 575 (1985).
- [11] G. Agazie *et al.* (NANOGrav), The NANOGrav 15 yr Data Set: Evidence for a Gravitational-wave Background, *Astrophys. J. Lett.* **951**, L8 (2023), [arXiv:2306.16213 \[astro-ph.HE\]](#).
- [12] A. Afzal *et al.*, The nanograv 15 yr data set: Search for signals from new physics, *The Astrophysical Journal Letters* **951**, L11 (2023).
- [13] P. Amaro-Seoane *et al.*, Laser interferometer space antenna (2017), [arXiv:1702.00786 \[astro-ph.IM\]](#).
- [14] K. Yagi and N. Seto, Detector configuration of DECIGO/BBO and identification of cosmological neutron-star binaries, *Phys. Rev. D* **83**, 044011 (2011), [Erratum: *Phys.Rev.D* 95, 109901 (2017)], [arXiv:1101.3940 \[astro-ph.CO\]](#).
- [15] M. Sasaki, T. Suyama, T. Tanaka, and S. Yokoyama, Primordial black holes—perspectives in gravitational wave astronomy, *Classical and Quantum Gravity* **35**, 063001 (2018).
- [16] B. Carr and F. Kühnel, Primordial black holes as dark matter: Recent developments, *Annual Review of Nuclear and Particle Science* **70**, 355–394 (2020).
- [17] A. M. Green and B. J. Kavanagh, Primordial black holes as a dark matter candidate, *Journal of Physics G: Nuclear and Particle Physics* **48**, 043001 (2021).
- [18] A. Escrivà, F. Kühnel, and Y. Tada, Primordial black holes (2023), [arXiv:2211.05767 \[astro-ph.CO\]](#).
- [19] O. Özsoy and G. Tasinato, Inflation and primordial black holes, *Universe* **9**, 203 (2023).
- [20] P. Villanueva-Domingo, O. Mena, and S. Palomares-Ruiz, A brief review on primordial black holes as dark matter, *Frontiers in Astronomy and Space Sciences* **8**, 10.3389/fspas.2021.681084 (2021).
- [21] H. Di and Y. Gong, Primordial black holes and second order gravitational waves from ultra-slow-roll inflation, *Journal of Cosmology and Astroparticle Physics* **2018** (07), 007.
- [22] S. Clesse, J. García-Bellido, and S. Orani, Detecting the stochastic gravitational wave background from primordial black hole formation (2018), [arXiv:1812.11011 \[astro-ph.CO\]](#).
- [23] N. Bartolo, V. D. Luca, G. Franciolini, A. Lewis, M. Peloso, and A. Riotto, Primordial black hole dark matter: LISA serendipity, *Physical Review Letters* **122**, 10.1103/physrevlett.122.211301 (2019).
- [24] F. Hajkarim and J. Schaffner-Bielich, Thermal history of the early universe and primordial gravitational waves from induced scalar perturbations, *Physical Review D* **101**, 10.1103/physrevd.101.043522 (2020).
- [25] J. Liu, Z.-K. Guo, and R.-G. Cai, Analytical approximation of the scalar spectrum in the ultraslow-roll inflationary models, *Physical Review D* **101**, 10.1103/physrevd.101.083535 (2020).
- [26] G. Ballesteros, M. A. García, A. Pérez Rodríguez, M. Pierre, and J. Rey, Primordial black holes and gravitational waves from dissipation during inflation, *Journal of Cosmology and Astroparticle Physics* **2022** (12), 006.
- [27] S. Kawai and J. Kim, Primordial black holes and gravitational waves from nonminimally coupled supergravity inflation, *Physical Review D* **107**, 10.1103/physrevd.107.043523 (2023).
- [28] Y. Aldabergenov, A. Addazi, and S. V. Ketov, Primordial black holes from modified supergravity, *Eur. Phys. J. C* **80**, 917 (2020), [arXiv:2006.16641 \[hep-th\]](#).
- [29] S. Balaji, G. Domènech, and G. Franciolini, Scalar-induced gravitational wave interpretation of PTA data: the role of scalar fluctuation propagation speed, *JCAP* **10**, 041, [arXiv:2307.08552 \[gr-qc\]](#).
- [30] A. Ghoshal, A. Moursy, and Q. Shafi, Cosmological probes of grand unification: Primordial black holes and scalar-induced gravitational waves, *Phys. Rev. D* **108**, 055039 (2023), [arXiv:2306.04002 \[hep-ph\]](#).
- [31] A. Ghoshal and A. Strumia, Traversing a kinetic pole during inflation: primordial black holes and gravitational waves, (2023), [arXiv:2311.16236 \[hep-ph\]](#).
- [32] W. Qin, S. R. Geller, S. Balaji, E. McDonough, and D. I. Kaiser, Planck constraints and gravitational wave forecasts for primordial black hole dark matter seeded by multifield inflation, *Phys. Rev. D* **108**, 043508 (2023), [arXiv:2303.02168 \[astro-ph.CO\]](#).
- [33] N. Ijaz, M. Mehmood, and M. U. Rehman, The Stochastic Gravitational-Wave Background from Primordial Black Holes in R-Symmetric $SU(5)$ Inflation, (2023), [arXiv:2308.14908 \[astro-ph.CO\]](#).
- [34] G. R. Dvali, Q. Shafi, and R. K. Schaefer, Large scale structure and supersymmetric inflation without fine tuning, *Phys. Rev. Lett.* **73**, 1886 (1994), [arXiv:hep-ph/9406319](#).
- [35] E. J. Copeland, A. R. Liddle, D. H. Lyth, E. D. Stewart, and D. Wands, False vacuum inflation with Einstein gravity, *Phys. Rev. D* **49**, 6410 (1994), [arXiv:astro-ph/9401011](#).
- [36] A. D. Linde and A. Riotto, Hybrid inflation in supergravity, *Phys. Rev. D* **56**, R1841 (1997), [arXiv:hep-ph/9703209](#).
- [37] V. N. Senoguz and Q. Shafi, Reheat temperature in supersymmetric hybrid inflation models, *Phys. Rev. D* **71**, 043514 (2005), [arXiv:hep-ph/0412102](#).
- [38] W. Buchmuller, L. Covi, and D. Delepine, Inflation and supersymmetry breaking, *Phys. Lett. B* **491**, 183 (2000), [arXiv:hep-ph/0006168](#).
- [39] M. U. Rehman, Q. Shafi, and J. R. Wickman, Supersymmetric Hybrid Inflation Redux, *Phys. Lett. B* **683**, 191 (2010), [arXiv:0908.3896 \[hep-ph\]](#).
- [40] V. N. Senoguz and Q. Shafi, Testing supersymmetric grand unified models of inflation, *Phys. Lett. B* **567**, 79 (2003), [arXiv:hep-ph/0305089](#).

- [41] V. C. Spanos and I. D. Stamou, Gravitational waves and primordial black holes from supersymmetric hybrid inflation, *Phys. Rev. D* **104**, 123537 (2021), [arXiv:2108.05671 \[astro-ph.CO\]](#).
- [42] S. Khalil, M. U. Rehman, Q. Shafi, and E. A. Zaakouk, Inflation in Supersymmetric SU(5), *Phys. Rev. D* **83**, 063522 (2011), [arXiv:1010.3657 \[hep-ph\]](#).
- [43] M. U. Rehman, M. M. A. Abid, and A. Ejaz, New Inflation in Supersymmetric SU(5) and Flipped SU(5) GUT Models, *JCAP* **11**, 019, [arXiv:1804.07619 \[hep-ph\]](#).
- [44] A. Pal and Q. Shafi, Supersymmetric $SU(5) \times U(1)_X$ and the weak gravity conjecture, *Phys. Rev. D* **100**, 043526 (2019), [arXiv:1903.05703 \[hep-ph\]](#).
- [45] W. Ahmed, M. U. Rehman, and U. Zubair, Probing stochastic gravitational wave background from $su(5) \times u(1)_X$ strings in light of nanograv 15-year data (2023), [arXiv:2308.09125 \[hep-ph\]](#).
- [46] A. Afzal, M. Mehmood, M. U. Rehman, and Q. Shafi, Supersymmetric hybrid inflation and metastable cosmic strings in $SU(4)_c \times SU(2)_L \times U(1)_R$, (2023), [arXiv:2308.11410 \[hep-ph\]](#).
- [47] B. Kyae and Q. Shafi, Inflation with realistic supersymmetric SO(10), *Phys. Rev. D* **72**, 063515 (2005), [arXiv:hep-ph/0504044](#).
- [48] G. R. Dvali, G. Lazarides, and Q. Shafi, Mu problem and hybrid inflation in supersymmetric SU(2)-L x SU(2)-R x U(1)-(B-L), *Phys. Lett. B* **424**, 259 (1998), [arXiv:hep-ph/9710314](#).
- [49] M. U. Rehman, Q. Shafi, and J. R. Wickman, Minimal Supersymmetric Hybrid Inflation, Flipped SU(5) and Proton Decay, *Phys. Lett. B* **688**, 75 (2010), [arXiv:0912.4737 \[hep-ph\]](#).
- [50] M. Civatelli, M. Ur Rehman, E. Sabo, Q. Shafi, and J. Wickman, R-symmetry breaking in supersymmetric hybrid inflation, *Phys. Rev. D* **88**, 103514 (2013), [arXiv:1303.3602 \[hep-ph\]](#).
- [51] M. U. Rehman, Q. Shafi, and U. Zubair, Gravity waves and proton decay in a flipped SU(5) hybrid inflation model, *Phys. Rev. D* **97**, 123522 (2018), [arXiv:1804.02493 \[hep-ph\]](#).
- [52] M. M. A. Abid, M. Mehmood, M. U. Rehman, and Q. Shafi, Realistic inflation in no-scale U(1) R symmetric flipped SU(5), *JCAP* **10**, 015, [arXiv:2107.05678 \[hep-ph\]](#).
- [53] A. Afzal, W. Ahmed, M. U. Rehman, and Q. Shafi, μ -hybrid inflation, gravitino dark matter, and stochastic gravitational wave background from cosmic strings, *Phys. Rev. D* **105**, 103539 (2022), [arXiv:2202.07386 \[hep-ph\]](#).
- [54] M. U. Rehman, Q. Shafi, and F. K. Vardag, μ -Hybrid Inflation with Low Reheat Temperature and Observable Gravity Waves, *Phys. Rev. D* **96**, 063527 (2017), [arXiv:1705.03693 \[hep-ph\]](#).
- [55] H. M. Lee, Chaotic inflation in Jordan frame supergravity, *Journal of Cosmology and Astroparticle Physics* **2010** (08), 003–003.
- [56] D. I. Kaiser, Conformal transformations with multiple scalar fields, *Physical Review D* **81**, 10.1103/physrevd.81.084044 (2010).
- [57] D. I. Kaiser, E. A. Mazenc, and E. I. Sfakianakis, Primordial bispectrum from multifield inflation with non-minimal couplings, *Physical Review D* **87**, 10.1103/physrevd.87.064004 (2013).
- [58] C. M. Peterson and M. Tegmark, Testing two-field inflation, *Physical Review D* **83**, 10.1103/physrevd.83.023522 (2011).
- [59] C. Gordon, D. Wands, B. A. Bassett, and R. Maartens, Adiabatic and entropy perturbations from inflation, *Physical Review D* **63**, 10.1103/physrevd.63.023506 (2000).
- [60] T. T. Nakamura and E. D. Stewart, The spectrum of cosmological perturbations produced by a multi-component inflaton to second order in the slow-roll approximation, *Physics Letters B* **381**, 413 (1996).
- [61] J.-O. Gong and T. Tanaka, A covariant approach to general field space metric in multi-field inflation, *Journal of Cosmology and Astroparticle Physics* **2011** (03), 015.
- [62] S. R. Geller, W. Qin, E. McDonough, and D. I. Kaiser, Primordial black holes from multifield inflation with non-minimal couplings, *Phys. Rev. D* **106**, 063535 (2022), [arXiv:2205.04471 \[hep-th\]](#).
- [63] M. A. Masoud, M. U. Rehman, and M. M. A. Abid, Non-minimal inflation in supersymmetric GUTs with $U(1)_R \times Z_n$ symmetry, *Int. J. Mod. Phys. D* **28**, 2040015 (2019), [arXiv:1910.10519 \[hep-ph\]](#).
- [64] Y. Akrami *et al.*, Planck2018 results: X. constraints on inflation, *Astron. Astrophys.* **641**, A10 (2020).
- [65] M. Dias, J. Frazer, and D. Seery, Computing observables in curved multifield models of inflation—A guide (with code) to the transport method, *JCAP* **12**, 030, [arXiv:1502.03125 \[astro-ph.CO\]](#).
- [66] D. J. Mulryne, D. Seery, and D. Wesley, Moment transport equations for non-gaussianity, *Journal of Cosmology and Astroparticle Physics* **2010** (01), 024–024.
- [67] D. J. Mulryne, D. Seery, and D. Wesley, Moment transport equations for the primordial curvature perturbation, *Journal of Cosmology and Astroparticle Physics* **2011** (04), 030–030.
- [68] S. Bird, H. V. Peiris, M. Viel, and L. Verde, Minimally parametric power spectrum reconstruction from the Lyman α forest, *Monthly Notices of the Royal Astronomical Society* **413**, 1717 (2011).
- [69] D. J. Fixsen, E. S. Cheng, J. M. Gales, J. C. Mather, R. A. Shafer, and E. L. Wright, The cosmic microwave background spectrum from the full COBE FIRAS data set, *The Astrophysical Journal* **473**, 576–587 (1996).
- [70] A. Baur, M. A. G. Garcia, R. Henriquez-Ortiz, M. Hernandez-Neri, and S. Ramos-Sanchez, Spectral distortions from promising single and multifield inflationary models, (2023), [arXiv:2310.13071 \[astro-ph.CO\]](#).
- [71] P. A. R. Ade *et al.* (BICEP, Keck), Improved Constraints on Primordial Gravitational Waves using Planck, WMAP, and BICEP/Keck Observations through the 2018 Observing Season, *Phys. Rev. Lett.* **127**, 151301 (2021), [arXiv:2110.00483 \[astro-ph.CO\]](#).
- [72] R. Laureijs *et al.* (EUCLID), Euclid Definition Study Report, (2011), [arXiv:1110.3193 \[astro-ph.CO\]](#).
- [73] P. Ade *et al.* (Simons Observatory), The Simons Observatory: Science goals and forecasts, *JCAP* **02**, 056, [arXiv:1808.07445 \[astro-ph.CO\]](#).
- [74] M. Hazumi *et al.* (LiteBIRD), LiteBIRD: JAXA's new strategic L-class mission for all-sky surveys of cosmic microwave background polarization, *Proc. SPIE Int. Soc. Opt. Eng.* **11443**, 114432F (2020), [arXiv:2101.12449 \[astro-ph.IM\]](#).
- [75] S. Y. Khlebnikov and M. E. Shaposhnikov, The Statistical Theory of Anomalous Fermion Number Nonconservation, *Nucl. Phys. B* **308**, 885 (1988).
- [76] J. A. Harvey and M. S. Turner, Cosmological baryon and lepton number in the presence of electroweak fermion

- number violation, *Phys. Rev. D* **42**, 3344 (1990).
- [77] B. J. Carr, **The Primordial black hole mass spectrum** (1975).
- [78] S. Young, C. T. Byrnes, and M. Sasaki, Calculating the mass fraction of primordial black holes, *Journal of Cosmology and Astroparticle Physics* **2014** (07), 045.
- [79] T. Harada, C.-M. Yoo, and K. Kohri, Threshold of primordial black hole formation, *Physical Review D* **88**, 10.1103/physrevd.88.084051 (2013).
- [80] I. Musco, J. C. Miller, and A. G. Polnarev, Primordial black hole formation in the radiative era: investigation of the critical nature of the collapse, *Classical and Quantum Gravity* **26**, 235001 (2009).
- [81] I. Musco, J. C. Miller, and L. Rezzolla, Computations of primordial black-hole formation, *Classical and Quantum Gravity* **22**, 1405 (2005).
- [82] A. Escrivà, C. Germani, and R. K. Sheth, Universal threshold for primordial black hole formation, *Physical Review D* **101**, 10.1103/physrevd.101.044022 (2020).
- [83] A. Escrivà, C. Germani, and R. K. Sheth, Analytical thresholds for black hole formation in general cosmological backgrounds, *Journal of Cosmology and Astroparticle Physics* **2021** (01), 030.
- [84] I. Musco, V. D. Luca, G. Franciolini, and A. Riotto, Threshold for primordial black holes. II. a simple analytic prescription, *Physical Review D* **103**, 10.1103/physrevd.103.063538 (2021).
- [85] B. J. Carr, K. Kohri, Y. Sendouda, and J. Yokoyama, New cosmological constraints on primordial black holes, *Physical Review D* **81**, 10.1103/physrevd.81.104019 (2010).
- [86] B. Carr, K. Kohri, Y. Sendouda, and J. Yokoyama, Constraints on primordial black holes, *Reports on Progress in Physics* **84**, 116902 (2021).
- [87] L. Badurina *et al.*, Aion: an atom interferometer observatory and network, *Journal of Cosmology and Astroparticle Physics* **2020** (05), 011–011.
- [88] Y. A. El-Neaj *et al.*, Aedge: Atomic experiment for dark matter and gravity exploration in space, *EPJ Quantum Technology* **7**, 10.1140/epjqt/s40507-020-0080-0 (2020).
- [89] H. Kudoh, A. Taruya, T. Hiramatsu, and Y. Himemoto, Detecting a gravitational-wave background with next-generation space interferometers, *Physical Review D* **73**, 10.1103/physrevd.73.064006 (2006).
- [90] S. Kawamura *et al.*, Current status of space gravitational wave antenna decigo and b-decigo (2020), [arXiv:2006.13545 \[gr-qc\]](https://arxiv.org/abs/2006.13545).
- [91] G. M. Harry, P. Fritschel, D. A. Shaddock, W. Folkner, and E. S. Phinney, Laser interferometry for the big bang observer, *Classical and Quantum Gravity* **23**, 4887 (2006).
- [92] A. Sesana *et al.*, Unveiling the gravitational universe at μ -hz frequencies, *Experimental Astronomy* **51**, 1333–1383 (2021).
- [93] P. E. Dewdney, P. J. Hall, R. T. Schilizzi, and T. J. L. W. Lazio, The square kilometre array, *Proceedings of the IEEE* **97**, 1482 (2009).
- [94] G. Janssen *et al.*, Gravitational Wave Astronomy with the SKA, *PoS AASKA14*, 037 (2015).
- [95] M. Maggiore, Gravitational wave experiments and early universe cosmology, *Physics Reports* **331**, 283 (2000).
- [96] D. Baumann, P. Steinhardt, K. Takahashi, and K. Ichiki, Gravitational wave spectrum induced by primordial scalar perturbations, *Physical Review D* **76**, 10.1103/physrevd.76.084019 (2007).
- [97] K. Kohri and T. Terada, Semianalytic calculation of gravitational wave spectrum nonlinearly induced from primordial curvature perturbations, *Physical Review D* **97**, 10.1103/physrevd.97.123532 (2018).
- [98] K. Inomata, M. Kawasaki, K. Mukaida, Y. Tada, and T. T. Yanagida, Inflationary primordial black holes for the LIGO gravitational wave events and pulsar timing array experiments, *Physical Review D* **95**, 10.1103/physrevd.95.123510 (2017).
- [99] K. Ando, K. Inomata, and M. Kawasaki, Primordial black holes and uncertainties in the choice of the window function, *Physical Review D* **97**, 10.1103/physrevd.97.103528 (2018).